Available online at www.sciencedirect.com
SCIENCE DIRECT®

Journal of the European Ceramic Society 23 (2003) 2639–2645
www.elsevier.com/locate/jeurceramsoc

# Composition dependence of the lattice vibrations in $Sr_{n+1}Ti_nO_{3n+1}$ Ruddlesden–Popper homologous series

S. Kamba[a,*], P. Samoukhina[a], F. Kadlec[a], J. Pokorný[a], J. Petzelt[a], I.M. Reaney[b], P.L. Wise[b]

[a]*Institute of Physics, Academy of Sciences of the Czech Republic, Na Slovance 2, 182 21 Prague 8, Czech Republic*
[b]*University of Sheffield, Department of Engineering Materials, Sheffield S1 3JD, UK*

**Abstract**

Room-temperature infrared reflectivities, time-domain THz transmission spectra and micro-Raman spectra of ceramics in the Ruddlesden–Popper homologous series, $Sr_{n+1}Ti_nO_{3n+1}$ (where $n=1$, 2, 3, 4, $\infty$), were studied. Increasing the number of perovskite layers ($n$) in the crystal system resulted in higher polarizability of the lattice and softening of the lowest frequency phonon mode, which is responsible for the observed increase in microwave permittivity, dielectric loss and temperature coefficient of resonance frequency with $n$. Although the infrared and Raman spectra revealed many defects in the ceramics (e.g. second phases and stacking faults), the extrapolation of experimental submillimetre dielectric data to the microwave region showed no dielectric dispersion below the phonon frequencies and prevailingly an intrinsic origin of losses in the microwave region in almost all samples (except for $Sr_5Ti_4O_{13}$).


*Keywords:* Dielectric properties; Perovskites; Spectroscopy

## 1. Introduction

Ruddlesden–Popper (RP) compounds[1,2] have the general formula $A_{n+1}B_nO_{3n+1}$ and are composed of $n$ perovskite blocks separated and sheared by rock-salt structured layers along $\frac{1}{2}$[111] (see Fig. 1). A large number RP compounds have been intensively studied because they exhibit useful properties such as high-temperature superconductivity, colossal magnetoresistance[3] or high dielectric permittivity. For Sr and Ca titanates, RP compounds may be formed by the addition of excess SrO and CaO to $SrTiO_3$ and $CaTiO_3$, respectively. For Sr-based compositions, solid state techniques have been successful in preparing polycrystalline samples only with $n=1$–3 and $\infty$ (i.e. $SrTiO_3$).[1,2,4] whereas for Ca based RP phases only $Ca_{n+1}Ti_nO_{3n+1}$ with $n=2,3$ and $\infty$ have been reported. Lattice energy calculations performed by several groups have shown that $Sr_3Ti_2O_7$ in the SrO–$SrTiO_3$ series is the most stable of the RP compounds and that there is no driving force to form single-phase samples with higher $n$.[5–8] However, very recent papers[9,10] have reported the successful growth of $Sr_{n+1}Ti_nO_{3n+1}$ epitaxial layers by reactive molecular beam epitaxy with $1\leqslant n\leqslant 5$. The films with $n\leqslant 3$ were nearly free of intergrowths, while $Sr_5Ti_4O_{13}$ and $Sr_6Ti_5O_{16}$ thin films contain noticeably more 'out of phase' boundaries in their perovskite sheets as well as intergrowth defects.[10] The number of perovskite layers controls the value of permittivity $\varepsilon'$ of the system; $Sr_2TiO_4$ has $\varepsilon'=37$, $Sr_5Ti_4O_{13}$ shows $\varepsilon'=100$ and the end member of the series, $SrTiO_3$, exhibits $\varepsilon'=290$.[11–13] The ability to control permittivity and loss by adjusting the SrO:$SrTiO_3$ ratio (varying the value of $n$)[11–13] makes $Sr_{n+1}Ti_nO_{3n+1}$ compounds candidates for microwave (MW) resonators and also for alternative gate oxides in MOSFETs. Furthermore, $Sr_{n+1}Ti_nO_{3n+1}$ ($1\leqslant n\leqslant 4$) ceramics were recently investigated and it was shown that the temperature coefficient of the resonant frequency (TCF) may be tuned close to zero by replacing Sr with Ca.[11–13]

The crystal structure of $Sr_{n+1}Ti_nO_{3n+1}$ ($n\leqslant 5$), schematically shown in Fig. 1, is tetragonal (space group I4/mmm–$D_{4h}^{17}$, $Z=2$), while the structure of $Ca_{n+1}Ti_nO_{3n+1}$ is orthorhombic.[1,2,14] As the number of perovskite layers ($n$) increases, only the c-parameter of the lattice

* Corresponding author.

0955-2219/03/$ - see front matter 
doi:10.1016/S0955-2219(03)00150-X

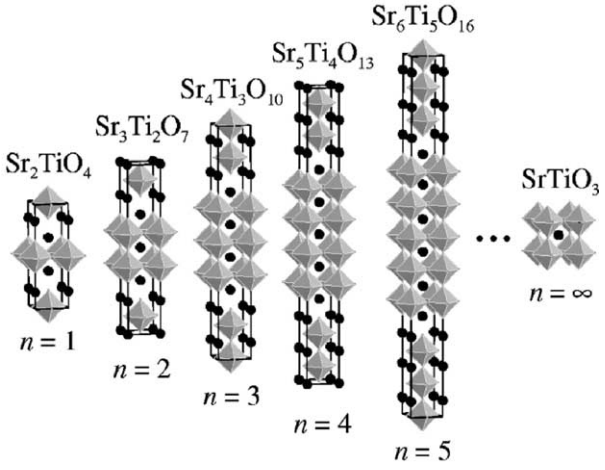


Fig. 1. Structure of the $Sr_{n+1}Ti_nO_{3n+1}$ unit cell of the RP homologous series for $n \in (1, 2, 3, 4, 5, \infty)$. Circles represent the Sr atoms, Ti atoms are at the centers of the octahedra with the oxygen atoms at each apex. (after Ref. 9).

increases. For the end member ($n=\infty$) of the Sr series, $SrTiO_3$, the structure transforms to the cubic symmetry ($Pm\bar{3}m-O_h^1$, $Z=1$) with only one perovskite layer.

The question of why the permittivity in $Sr_{n+1}Ti_nO_{3n+1}$ RP homologous series increases with the number of perovskite layers has not yet been studied other than by considering the compositions as simple mixtures of SrO and $SrTiO_3$, i.e. the greater the concentration of $SrTiO_3$ (increase in $n$) the higher the permittivity.[11–13] It is known that the polar phonons are responsible for the high static permittivity in $SrTiO_3$ (i.e. no dielectric dispersion occurs below the phonon frequencies) and that the softening of the polar soft mode on cooling is responsible for its incipient ferroelectric behaviour, i.e. the dramatic increase of $\varepsilon'$ on cooling.[15] Polar optical modes can be conveniently studied by using infrared (IR) spectroscopy and it is the aim of this paper to compare already published IR reflectivity spectra of $SrTiO_3$[15] with $Sr_{n+1}Ti_nO_{3n+1}$ ($1 \leqslant n \leqslant 4$) spectra with an accent on extrapolation of IR and submillimetre dielectric data down to the MW range. For completeness of the lattice dynamics study, micro-Raman spectra of $Sr_{n+1}Ti_nO_{3n+1}$ were also taken and compared with that of $SrTiO_3$ published in Ref. 15.

## 2. Experimental

The sample processing of $Sr_{n+1}Ti_nO_{3n+1}$ ($1 \leqslant n \leqslant 4$) ceramic pellets with diameter 16 mm and height 7 mm was described elsewhere.[11,12] X-ray diffraction data and transmission electron microscopy results together with MW data obtained on our samples were already published[11,12] and these results will be used for interpretation of our IR and Raman spectra.

Room-temperature IR reflectivity spectra in specular geometry were obtained using a Fourier transform spectrometer Bruker IFS 113v in the spectral range of 30–3000 $cm^{-1}$ (0.9–90 THz). Pyroelectric deuterated triglycine sulfate detectors with polyethylene and KBr windows were used below 700 and above 400 $cm^{-1}$, respectively.

A custom-made time-domain THz transmission spectrometer was used to obtain the complex dielectric response in the submillimetre frequency range from 10 to 55 $cm^{-1}$ (0.3–1.65 THz). This spectrometer uses 1-mJ femtosecond laser pulses to generate THz radiation via optical rectification on a ZnTe single crystal, and an electro-optic sampling detection technique. This measuring technique is described in detail elsewhere.[16] Polished plane-parallel 200 μm thick disks with a diameter of 16 mm were studied.

The micro-Raman spectra were excited with the 514.5 nm line of an Ar laser and recorded in the back-scattering geometry using a Renishaw Ramascope at room temperature. The low-frequency cutoff $\sim 60$ $cm^{-1}$ is determined by the notch filter which removes the strong elastically scattered light from the spectrum.

## 3. Results

Experimental IR reflectivity spectra of all investigated samples are shown in Fig. 2. The portion of the spectra above 1000 $cm^{-1}$ is not shown because no reflection bands were observed and the reflectivity levels off at a value determined by the high frequency permittivity $\varepsilon_\infty$ due to electron absorption processes in visible and UV range. The complex dielectric response $\varepsilon^*(\omega)=\varepsilon'(\omega)—i\,\varepsilon''(\omega)$ in the IR range can be obtained from the reflectivity $R(\omega)$ fit via

$$R(\omega) \equiv \left| \frac{\sqrt{\varepsilon^*(\omega)}-1}{\sqrt{\varepsilon^*(\omega)}+1} \right|^2 \tag{1}$$

and a generalized four-parameter damped oscillator model is used for the complex dielectric function.[17]

$$\varepsilon^*(\omega) = \varepsilon_\infty \prod_j \frac{\omega_{LOj}^2 - \omega^2 + i\omega\gamma_{LOj}}{\omega_{TOj}^2 - \omega^2 + i\omega\gamma_{TOj}}. \tag{2}$$

Here $\omega_{TOj}$ and $\omega_{LOj}$ denote transverse and longitudinal eigenfrequencies of the $j$-th polar phonon and $\gamma_{TOj}$ and $\gamma_{LOj}$ denote their respective damping constants. The resulting $\varepsilon'(\omega)$ and $\varepsilon''(\omega)$ spectra are shown in the broad spectral range in Fig. 3. The fitted mode parameters are listed in Table 1.

Micro-Raman spectra of all $Sr_{n+1}Ti_nO_{3n+1}$ ceramics are shown in Fig. 4. The spectra $I(\omega)$ were fitted with the sum of Gaussian curves

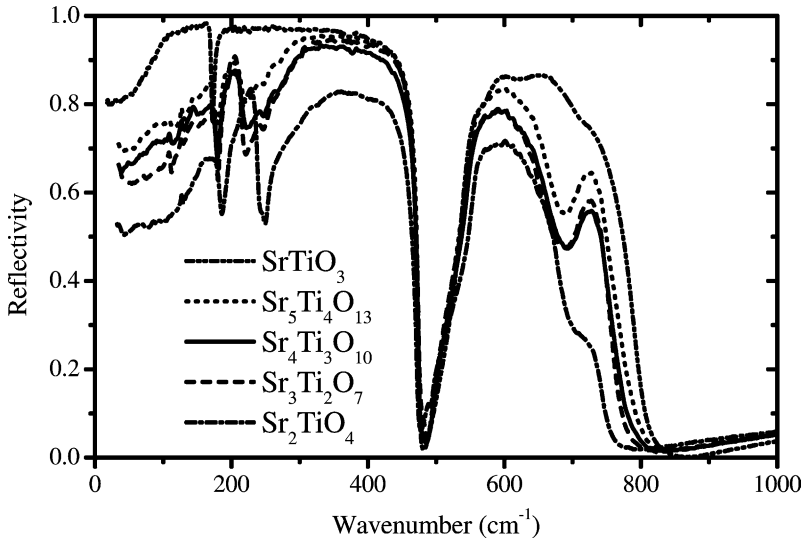


Fig. 2. IR reflectivity spectra of $Sr_{n+1}Ti_nO_{3n+1}$ ceramics for $n \in (1, 2, 3, 4, \infty)$. The spectrum of the $SrTiO_3$ ceramics is taken from Ref. 15.

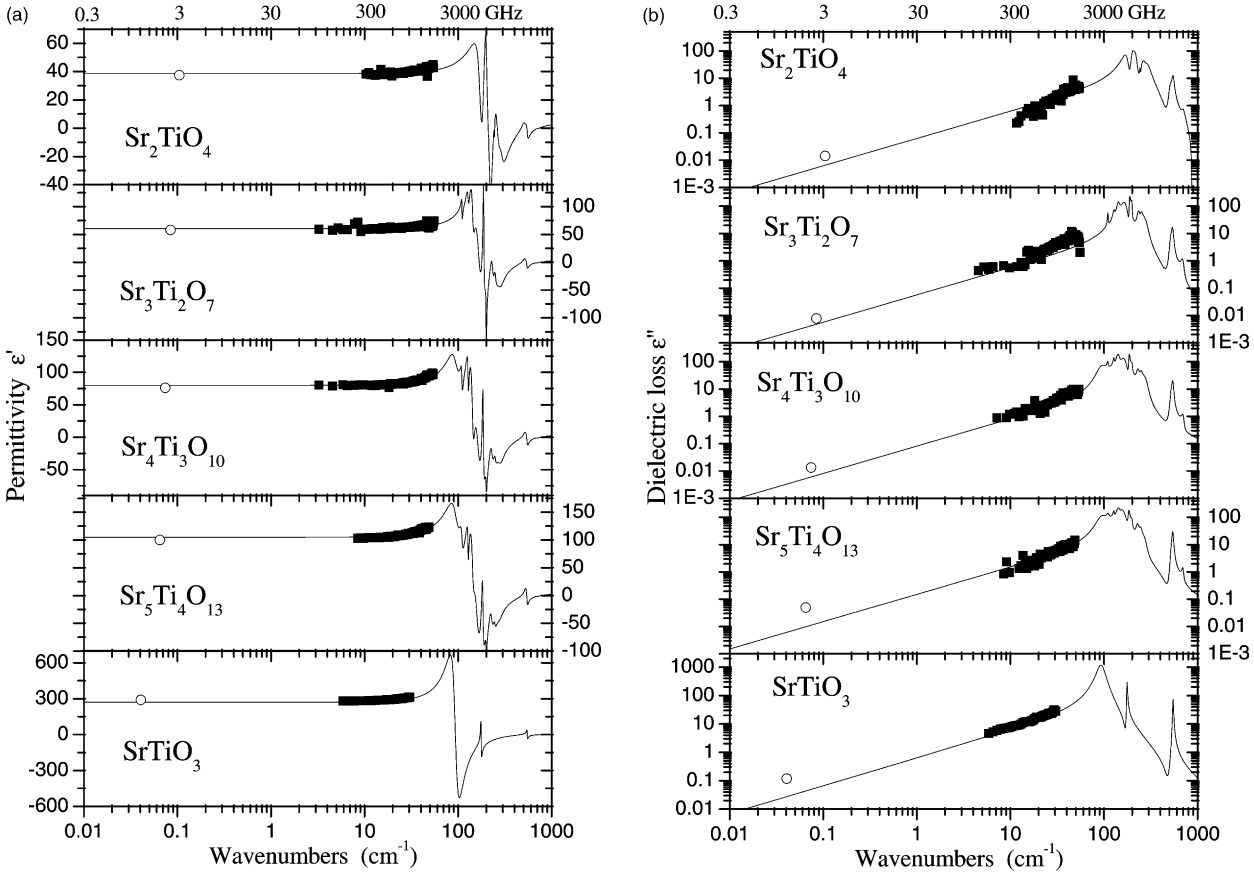


Fig. 3. Real (a) and imaginary (b) part of the dielectric function of $Sr_{n+1}Ti_nO_{3n+1}$ ceramics calculated from the fits to the IR reflectivities and experimental dielectric data (solid points) calculated from the time-domain THz transmission spectra. Open points show MW dielectric data from Refs. 11 and 12.

Table 1
List of parameters of the observed polar phonon modes in $Sr_{n+1}Ti_nO_{3n+1}$ ceramics

| No | $Sr_2TiO_4$ | | | $\varepsilon_\infty=4.5$ | | | $Sr_3Ti_2O_7$ | | $\varepsilon_\infty=4.7$ | | | $Sr_4Ti_3O_{10}$ | | $\varepsilon_\infty=4.7$ | | | $Sr_5Ti_4O_{13}$ | | $\varepsilon_=5.1$ | | | $SrTiO_3$ | | $\varepsilon_\infty=5.8$ | |
|---|---|---|---|---|---|---|---|---|---|---|---|---|---|---|---|---|---|---|---|---|---|---|---|---|---|
| | Assign | $\omega_{TOj}$ | $\gamma_{TOj}$ | $\omega_{LOj}$ | $\gamma_{LOj}$ | $\Delta\varepsilon_j$ | Assign | $\omega_{TOj}$ | $\gamma_{TOj}$ | $\omega_{LOj}$ | $\gamma_{LOj}$ | $\Delta\varepsilon_j$ | Assign | $\omega_{TOj}$ | $\gamma_{TOj}$ | $\omega_{LOj}$ | $\gamma_{LOj}$ | $\Delta\varepsilon_j$ | Assign | $\omega_{TOj}$ | $\gamma_{TOj}$ | $\omega_{LOj}$ | $\gamma_{LOj}$ | $\Delta\varepsilon_j$ |
| 1 | $TO_2$ | 177 | 31 | 184 | 9 | 9.0 | | 110.0 | 2.1 | 110.4 | 2.1 | 0.8 | | 94.1 | 27.0 | 100.5 | 31.7 | 15.1 | | 95.2 | 29.0 | 104.0 | 31.7 | 28.1 | $TO_1$ | 93.0 | 20.0 | 171.0 | 1.1 | 283.1 |
| 2 | $TO_1$ | 201 | 20.5 | 210 | 25 | 9.0 | | 128.0 | 5.9 | 128.7 | 5.9 | 1.6 | | 109.9 | 2.1 | 110.4 | 2.1 | 0.7 | | 109.9 | 4.1 | 111.1 | 4.1 | 1.5 | $TO_2$ | 176 | 3.0 | 472.0 | 2.0 | 6.2 |
| 3 | $TO_2$ | 218 | 22 | 239 | 10 | 6.5 | $TO_1$ | 142.8 | 12.0 | 146.5 | 13.7 | 8.1 | | 128.0 | 4.0 | 128.8 | 4.0 | 2.0 | | 128.0 | 4.0 | 128.8 | 4.0 | 2.3 | $TO_4$ | 548.0 | 11.0 | 795.0 | 35.0 | 1.7 |
| 4 | | 244.4 | 4 | 245.6 | 3.5 | 0.3 | $TO_1$ | 166.4 | 34.3 | 181.5 | 5.4 | 26.9 | $TO_1$ | 143.0 | 13.6 | 148.2 | 13.7 | 14.3 | $TO_1$ | 144.0 | 13.6 | 147.0 | 13.7 | 13.4 | | | | | | |
| 5 | | 257 | 41.7 | 470 | 14.4 | 6.2 | $TO_2$ | 187.5 | 6.0 | 199.0 | 9.2 | 8.1 | $TO_1$ | 162.1 | 37.2 | 180.2 | 5.4 | 28.3 | $TO_1$ | 157.1 | 37.2 | 179.0 | 7.0 | 40.4 | | | | | | |
| 6 | | 292 | 43.2 | 284.6 | 40.2 | 2.3 | | 199.4 | 4.4 | 221.4 | 16.5 | 0.4 | $TO_2$ | 185.0 | 6.7 | 199.0 | 9.2 | 6.8 | $TO_2$ | 183.4 | 8.3 | 199.0 | 9.2 | 7.2 | | | | | | |
| 7 | $TO_4$ | 510 | 49.3 | 529.3 | 49.3 | 0.4 | | 233.7 | 19.2 | 475.6 | 9.9 | 4.2 | | 199.6 | 6.7 | 221.5 | 17.8 | 0.6 | $TO_2$ | 199.6 | 7.0 | 221.2 | 17.8 | 0.6 | | | | | | |
| 8 | $TO_4$ | 547 | 32 | 686.3 | 52.3 | 0.5 | | 248.9 | 17.8 | 245.0 | 14.0 | 2.0 | | 228.7 | 20.6 | 475.6 | 12.2 | 3.1 | | 227.2 | 20.0 | 475.0 | 5.5 | 3.4 | | | | | | |
| 9 | | 701.5 | 64.7 | 743.7 | 41.7 | 0.03 | | 280.0 | 50.0 | 270.8 | 60.2 | 2.9 | | 249.0 | 15.0 | 246.6 | 15.0 | 0.8 | | 247.6 | 13.5 | 246.0 | 14.3 | 0.8 | | | | | | |
| 10 | | | | | | | $TO_4$ | 515.0 | 35.7 | 527.0 | 41.7 | 0.4 | | 280.0 | 50.0 | 270.8 | 63.2 | 2.4 | | 275.3 | 42.6 | 272.4 | 50.6 | 0.9 | | | | | | |
| 11 | | | | | | | $TO_4$ | 541.8 | 26.1 | 679.0 | 63.2 | 0.6 | $TO_4$ | 518.7 | 33.1 | 527.1 | 41.7 | 0.3 | $TO_4$ | 522.0 | 33.0 | 527.0 | 41.7 | 0.3 | | | | | | |
| 12 | | | | | | | | 697.1 | 55.4 | 757.2 | 20.5 | 0.06 | $TO_4$ | 543.7 | 26.1 | 690.8 | 63.2 | 0.7 | $TO_4$ | 543.7 | 23.0 | 689.7 | 42.0 | 1.0 | | | | | | |
| 13 | | | | | | | | | | | | | | 704.7 | 47.0 | 760.2 | 29.0 | 0.04 | | 698.5 | 34.6 | 774.3 | 34.6 | 0.04 | | | | | | |

Transverse $\omega_{TOj}$ and longitudinal $\omega_{LOj}$ frequencies and the corresponding dampings $\omega_{TOj}$ and $\omega_{LOj}$ are in $cm^{-1}$. Each triply degenerate $TO_j$ mode from $SrTiO_3$ splits into doublets.

$$I(\omega) = \sum_j I_{oj} e - \frac{(\omega - \omega_j)^2}{\gamma_j^2} + \text{const} \tag{3}$$

where $\omega_j$ and $\gamma_j$ mean the frequency of of the $j$-th Raman peak and its full with at half maximum, respectively. Fit parameters of Raman spectra are listed in Table 2.

## 4. Discussion

One can see in Fig. 2 that the low frequency reflectivity rises with the number of perovskite layers, $n$, in the $Sr_{n+1}Ti_nO_{3n+1}$ homologous series. This increase corresponds to the rise of the MW and submillimetre permittivity (see Fig. 3a) so that the growth of the MW $\varepsilon'$ is only due to contributions from polar phonons.

Let us discuss what can be obtained from IR and submillimetre data. The application of IR reflectivity for estimation of MW dielectric properties was first used by Wakino et al.,[18] who assumed that the intrinsic dielectric loss should obey the simple proportionality $\varepsilon'' \propto \omega$ in the GHz range. Their conclusion was based on the low-frequency limit of the sum of classical damped harmonic oscillators,[17] however this model which assumes

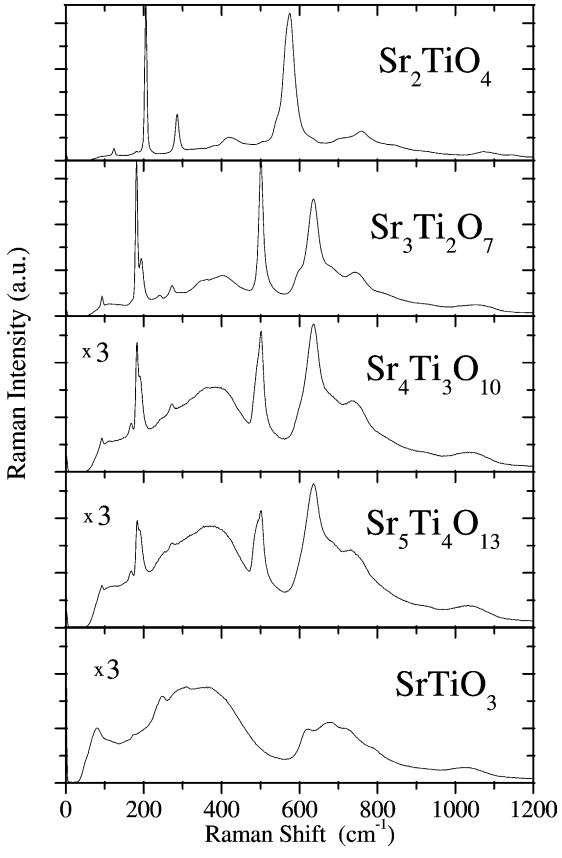


Fig. 4. Micro-Raman spectra of $Sr_{n+1}Ti_nO_{3n+1}$ ceramics. Note that the last three spectra were accumulated three times longer. The $SrTiO_3$ spectrum is taken from Ref. 15.

Table 2
List of parameters from the fits of micro-Raman spectra of $Sr_{n+1}Ti_nO_{3n+1}$ ceramics

| No | $Sr_2TiO_4$ | | | | $Sr_3Ti_2O_7$ | | | | $Sr_4Ti_3O_{10}$ | | | | $Sr_5Ti_4O_{13}$ | | | |
|---|---|---|---|---|---|---|---|---|---|---|---|---|---|---|---|---|
| | Comment | $\omega_j$ | $I_{oj}$ | $\gamma_j$ | Comment | $\omega_j$ | $I_{oj}$ | $\gamma_j$ | Comment | $\omega_j$ | $I_{oj}$ | $\gamma_j$ | Comment | $\omega_j$ | $I_{oj}$ | $\gamma_j$ |
| 1 | DI | 123.5 | 7.3 | 6.9 | DI | 93.3 | 10.5 | 5.3 | DI | 92.8 | 3.0 | 7.0 | DI | 91.9 | 8.2 | 9.3 |
| 2 | DI | 181.6 | 2.7 | 12.7 | 1st OS | 181.6 | 148.0 | 5.9 | DI | 167.4 | 4.0 | 8.3 | Background | 123.8 | 36.1 | 129.3 |
| 3 | 1st OS | 205.6 | 163.0 | 6.8 | DI | 193.3 | 45.0 | 15.0 | 1st OS | 182.3 | 23.6 | 5.7 | DI | 167.0 | 13.3 | 12.5 |
| 4 | 1st OS | 286.1 | 38.1 | 11.6 | DI | 239.8 | 3.4 | 10.7 | DI | 190.2 | 19.8 | 15.6 | DI | 182.3 | 30.4 | 5.7 |
| 5 | | 421.1 | 9.2 | 42.3 | 1st OS | 273.3 | 10.9 | 16.7 | Background | 229.9 | 12.5 | 305 | 1st OS | 189.5 | 53.6 | 17.6 |
| 6 | | 504.7 | 2.2 | 23.7 | | 357.8 | 13.2 | 68.1 | | 271.6 | 4.2 | 49.8 | | 260.2 | 56.9 | 127.8 |
| 7 | | 539.9 | 17.8 | 19.2 | | 410.0 | 13.5 | 49.2 | | 382.6 | 18.6 | 140.3 | | 271.9 | 5.2 | 8.9 |
| 8 | 1st OS | 573.3 | 14.0 | 32.0 | 1st OS | 501.4 | 133.0 | 14.5 | 1st OS | 498.1 | 29.3 | 26.3 | | 381.0 | 84.2 | 147.8 |
| 9 | Background | 574.6 | 15.7 | 551.4 | Background | 514.2 | 27.2 | 667.1 | | 502.0 | 9.7 | 6.9 | DI | 484.0 | 20.0 | 10.6 |
| 10 | | 615.8 | 10.6 | 38.7 | | 601.1 | 20.0 | 24.1 | 1st OS | 633.3 | 31.4 | 41.4 | 1st OS | 499.4 | 75.2 | 23.4 |
| 11 | | 711.9 | 6.1 | 46.3 | 1st OS | 634.4 | 88.2 | 29.7 | Background | 653.9 | 10.8 | 513.0 | 1st OS | 633.8 | 99.2 | 47.0 |
| 12 | | 759.0 | 11.8 | 40.6 | | 672.8 | 28.0 | 66.4 | | 705.5 | 14.5 | 152.8 | Background | 664.4 | 40.2 | 457.9 |
| 13 | | 804.5 | 6.0 | 142.7 | | 745.1 | 18.2 | 47.7 | | 1043.9 | 3.2 | 84.0 | | 681.2 | 18.6 | 28.6 |
| 14 | | 1078.9 | 4.5 | 56.1 | | 780.9 | 8.2 | 143.1 | | | | | | 727.0 | 38.7 | 107.0 |
| 15 | | 1143.7 | 1.7 | 41.6 | | 1055.7 | 5.8 | 86.7 | | | | | | 1042.3 | 11.0 | 91.1 |

$\omega_j$ and $\gamma_j$ parameters are in $cm^{-1}$, $I_{oj}$ is dimensionless. DI and 1st OS mean defect induced 1st order scattering and pure 1st order scattering, respectively. The rest of the modes (including broad backgrounds) have their origin in second order scattering (with a possible defect induced contribution).

frequency independent damping is valid only in the vicinity of phonon eigenfrequencies $\omega_{TOj}$, whereas the GHz range is 2–4 orders of magnitude below these frequencies. Nevertheless, the microscopic phonon transport theory[19–21] shows that in the MW range two-phonon difference decay processes dominate at room and medium-high temperatures (T) and that for the intrinsic loss spectrum, $\varepsilon'' \propto \omega T^2$. At low temperatures this T-dependence is not universal, but always much steeper.[19–21] This differs from the prediction based on damped oscillator model, where $\varepsilon'' \propto \omega T$. Most extrinsic sources of losses (with exception of charged point defects) show different frequency dependencies. In particular, they may cause dielectric relaxations with frequencies in the MW range or lower and, as a rule, do not contribute to $\varepsilon''$ in the submillimetre range.[21,22] Irrespective of their microscopic origin, the extrapolation of losses from submillimetre to MW using the simple $\varepsilon'' \propto \omega$ formula yields the upper estimate of the intrinsic MW losses. Therefore, the measurement of submillimetre dielectric response (and its temperature dependence) provides useful information about the origin of the MW response. We have shown that the evaluation of submillimetre dielectric response from the far-IR reflectivity is less accurate than from transmission measurements.[22–24] The most accurate is the complex transmittance measurement by the backward-wave-oscillator technique[25] or by the time-domain THz technique,[16] which enables a direct measurement of both $\varepsilon'(\omega)$ and $\varepsilon''(\omega)$, while far-IR spectrometers give only power transmission which must be model-fitted to obtain $\varepsilon^*(\omega)$. The time-domain THz transmission technique has the advantage compared with the backward-wave-oscillator technique, of providing results in a broader spectral range in a single run (our setup works in the range of 3–75 $cm^{-1}$, while backward-wave-oscillator technique uses a sequence of different sources and works below 40 $cm^{-1}$).

Our experimental submillimetre data (solid points in Fig. 3) agree, within experimental error, with the curves obtained from the reflectivity fits and the extrapolation to MW range agrees (with exception of $Sr_5Ti_4O_{13}$) with the experimental MW data (open points in Fig. 3). It means that no dielectric dispersion appears in the MW region which explains the high MW quality factor ($Q$). The validity of the relationship, $\varepsilon'' \propto \omega$, in the submillimetre and MW region demonstrates that intrinsic losses dominate in most samples ($Sr_5Ti_4O_{13}$ is the exception) and the processing of ceramics is, from the MW viewpoint, optimized.

In $Sr_{n+1}Ti_nO_{3n+1}$ ($n \leqslant 4$), a number of reflection bands with Raman peaks higher than in $SrTiO_3$ were observed. One possible reason for this observation is the tetragonal symmetry and larger unit cell of RP phases with respect to $SrTiO_3$, which is cubic (Fig. 1). The factor group analysis of lattice vibrations of all the studied compounds is summarized in Table 3. However, a higher number of modes was observed in IR and even more in the Raman spectra (Table 2) than predicted by the group theory. For example, in the Raman spectra of $Sr_2TiO_4$, 15 peaks were observed although only four modes are predicted. Some of the peaks may appear due to multiphonon scattering and absorption, but the disagreement with theory is so large that many of the peaks have to be defect induced. X-ray diffraction shows that practically all samples (with the exception of $Sr_3Ti_2O_7$) have traces of other phases.[11] The $n=4$ sample was shown to consist of phases with $n=1, 2, 3, \infty$ so that the

Table 3
Factor group analysis of the lattice vibrations in several $Sr_{n+1}Ti_nO_{3n+1}$ compounds

| Material | Factor group analysis |
|---|---|
| $Sr_2TiO_4$ | $3A_{2u}(IR)+4E_u(IR)+1B_{2u}+2A_{1g}(R)+2E_g(R)$ |
| $Sr_3Ti_2O_7$ | $5A_{2u}(IR)+6E_u(IR)+1B_{2u}+4A_{1g}(R)+1B_{1g}(R)+5E_g(R)$ |
| $Sr_4Ti_3O_{10}$ | $7A_{2u}(IR)+9E_u(IR)+2B_{2u}+6A_{1g}(R)+1B_{1g}(R)+7E_g(R)$ |
| $SrTiO_3$ | $3F_{1u}(IR)+1F_{2u}$ |

Acoustic modes ($1A_{2u}+1E_u$ in the tetragonal samples and $1F_{1u}$ in the cubic $SrTiO_3$) are not included. IR and Raman activity is parenthesised. $B_{2u}$ and $F_{2u}$ modes are silent. The analysis was not performed for $Sr_5Ti_4O_{13}$ because its crystal structure was not precisely determined and the sample was multiphase.

marker $n=4$ is used only because the composition corresponds effectively to $Sr_5Ti_4O_{13}$. Transmission electron microscopy studies directly revealed a large degree of one-dimensional disorder along the c-axis, equivalent to the presence of intergrowths of different homologue phases up to $n=20$.[10,12] Stacking faults like these can cause activation of phonons from outside of the Brillouin zone center. For example, sharp peaks below 150 $cm^{-1}$ in IR and Raman spectra are probably activated acoustic modes caused by folding of the Brillouin zone. The strongly multiphase composition of $Sr_5Ti_4O_{13}$ is probably responsible for breaking of the linear frequency dependence of $\varepsilon''(\omega)$. The reason why this is not the case in other samples is the small concentration of second phase.[10,11] In $Sr_4Ti_3O_{10}$ a smaller number of Raman peaks were observed than allowed from group theory, probably due to their low intensity and possible overlapping. Nevertheless, some of the peaks still have second-order or defect induced origins. Notice that no Raman active modes are permitted in $SrTiO_3$, however, several peaks are seen in Fig. 4 which were assigned by the authors of Ref. 15 to two-phonon scattering.

In IR spectra of $SrTiO_3$ only three IR active modes were observed in agreement with factor group analysis. The first mode with the lowest frequency (usually denoted as $TO_1$) corresponds mainly to a stretching vibration inside the octahedra (Ti against O), the second mode $TO_2$ is a translation vibration of Sr against $TiO_6$ octahedra. The $TO_3$ mode concerns rotations of oxygen atoms and is silent. The last mode, denoted as $TO_4$, is an oxygen bending vibration.[26] Notice that in all other MW (non-ferroelectric) perovskite ceramics the assignment of the first two modes is reversed. Softening of the $TO_1$ mode on cooling is responsible for the incipient ferroelectric behaviour of $SrTiO_3$ (i.e. increase in the permittivity at low temperatures up to $10^4$). The analysis of Fig. 2 and Table 1 shows that the strongest $TO_1$ mode is composition dependent and its frequency softens from 201 $cm^{-1}$ in $Sr_2TiO_4$ (in this case the frequency of $TO_1$ mode is higher than $TO_2$—as in other non-ferroelectric perovskites) to 157 $cm^{-1}$ in $Sr_5Ti_4O_{13}$ and it reaches the value 93 $cm^{-1}$ in $SrTiO_3$. Simultaneously, dielectric strength $\Delta\varepsilon_j$ of the most modes increases with the number of perovskite layers in the unit cell, which explains the increase in MW $\varepsilon'$ with $n$. The rise in the dielectric strength of polar phonons means that there is an increase in polarizability of the $Sr_{n+1}Ti_nO_{3n+1}$ lattice with $n$ which results in a systematic increases in the MW $\varepsilon''$ with $n$. This effect is a consequence of a softening of polar phonon frequencies (mainly of the $TO_1$ vibration). TCF depends on the temperature dependence of $\varepsilon'$, which is determined by variation of polar phonon frequencies with temperature. The lower the phonon frequency, the higher is its sensitivity to temperature change, or, in other words, the TCF is higher. In this manner the increase in TCF with the number of perovskite layers ($n$) may be explained.[12,13]

All the $F_{1u}$ modes in $SrTiO_3$ should split into $E_g$ and $A_{2u}$ doublets in $Sr_{n+1}Ti_nO_{3n+1}$ and their assignment is in Table 1. Other modes are not designated because their assignment is ambiguous. In $SrTiO_3$, the silent $TO_3$ mode lies in the region of $\sim$280 $cm^{-1}$.[15] Other strong polar modes are in the same spectral range but it is difficult to claim that these modes are split $TO_3$ vibrations (rotations of octahedra) since they can also be vibrations of SrO interlayers.

## 5. Conclusion

Lattice vibrations of $Sr_{n+1}Ti_nO_{3n+1}$ RP homologous series ($n=1,2,3,4,\infty$) were studied at room temperature by IR reflectivity, time-domain THz transmission spectroscopy and micro-Raman scattering. The rise of MW permittivity with the number of perovskite layers $n$ was explained by the increase in the dielectric strengths of polar phonons due to the higher polarizability of the crystal lattice. The increase in MW losses and TCF was explained by the decrease of the $TO_1$ vibration frequency with $n$. Linear extrapolation of the dielectric losses from the submillimetre to MW range agrees with the experimental values so that the dielectric losses are predominantly intrinsic and the sample processing was optimal for MW applications. Only for $Sr_5Ti_4O_{13}$ ceramics does the extrapolation $\varepsilon''(\omega)\omega$ not work suggesting that extrinsic losses are significant in this sample, probably due to its distinct multiphase composition.

## Acknowledgements

The work was supported by the Grant Agency of the Czech Republic (Projects Nos. 202/01/0612 and 203/99/0067) and by the Grant Agency of ASCR (Project No. A1010213).

## References


1. Ruddlesden, S. N. and Popper, P., New compounds of the $K_2NiF_2$ type. *Acta Crystall.*, 1957, **10**, 538–539.
2. Ruddlesden, S. N. and Popper, P., The compound $Sr_3Ti_2O_7$ and its structure. *Acta Crystall.*, 1958, **11**, 54–55.
3. Moritomo, Y., Asamitsu, A., Kuwahara, H. and Tokura, Y., Giant magnetoresistance of manganese oxides with a layered perovskite structure. *Nature (London)*, 1980, **380**, 141–144.
4. McCarthy, G. J., White, W. B. and Roy, R., Phase equilibria in the 1375 °C isotherm of the system Sr-Ti-O. *J. Am. Ceram. Soc.*, 1969, **52**, 463–469.
5. Udayakumar, K. R. and Cormack, A. N., Structural aspects of phase-equilibria in the Strontium-Titanium-Oxygen system. *J. Am. Ceram. Soc.*, 1988, **71**, C469–C471.
6. Udayakumar, K. R. and Cormack, A. N., Non-stoichiometry in alkaline-earth excess alkaline-earth titanates. *J. Phys. Chem. Solids*, 1989, **50**, 55–60.
7. Grimes, R. W., McCoy, M. A. and Lee, W. E., Phase stability and interfacial structures in the SrO-$SrTiO_3$ system. *Philos. Mag.*, 1997, **A75**, 833–846.
8. Noguera, C., Theoretical investigation of the Ruddlesden–Popper compounds $Sr_{n+1}Ti_nO_{3n+1}$ ($n=1$–3). *Philos. Mag. Lett.*, 2000, **80**, 173–180.
9. Haeni, J. H., Theis, C. D., Schlom, D. G., Tian, W., Pan, X. Q., Chang, H., Takeuchi, I. and Xiang, X.-D., Epitaxial growth of the first five members of the $Sr_{n+1}Ti_nO_{3n+1}$ Ruddlesden–Popper homolobous series. *Appl. Phys. Lett.*, 2001, **78**, 3292–3294.
10. Tian, W., Pan, X. Q., Haeni, J. H. and Schlom, D. G., Transmission electron microscopy study of $n=1$–5 $Sr_{n+1}Ti_nO_{3n+1}$ epitaxial thin films. *J. Mater. Res.*, 2001, **16**, 2013–2026.
11. Wise, P. L., Reaney, I. M., Lee, W. E., Price, T. J., Iddles, D. M. and Cannell, D. S., Structure-microwave property relations in $(Sr_xCa_{(1-x)})_{n+1}Ti_nO_{3n+1}$. *J. Eur. Ceram. Soc.*, 2001, **21**, 1723–1726.
12. Wise, P. L., Reaney, I. M., Lee, W. E., Price, T. J., Iddles, D. M. and Cannell, D. S., Structure-microwave property relations of Ca and Sr titanates. *J. Eur. Ceram. Soc.*, 2001, **21**, 2629–2632.
13. Reaney, I. M., Wise, P. L., Lee, W. E., Iddless, D. M., Cannell, D. S. and Price, T. J. Tunability of TCF in Ruddlesden–Popper compounds. *Proceedings of the 12th IEEE International Symposium on the Applications of Ferroelectrics* (ISAF 2000), 2001, IEEE 00CH37076, 187–190.
14. Elcombe, M. M., Kisi, E. H., Hawkins, K. D., White, T. J., Goodman, P. and Matheson, S., Structure determinations for $Ca_3Ti_2O_7$, $Ca_4Ti_3O_{10}$, $Ca_{3.6}Sr_{0.4}Ti_3O_{10}$ and a refinement of $Sr_3Ti_2O_7$. *Acta. Cryst.*, 1991, **B47**, 305–314.
15. Petzelt, J., Ostapchuk, T., Gregora, I., Rychetsky, I., Hoffmann-Eifert, S., Pronin, A. V., Yuzyuk, Y., Gorshunov, B. P., Kamba, S., Bovtun, V., Pokorny, J., Savinov, M., Porokhonskyy, V., Rafaja, D., Vanek, P., Almeida, A., Chaves, M.R., Volkov, A. A., Dressel, M., and Waser, R., Dielectric, infrared and Raman response of undoped $SrTiO_3$ ceramics: evidence of polar grain boundaries. *Phys. Rev.* 2001, B64, 184111/1-10 and references therein.
16. Kuzel, P. and Petzelt, J., Time-resolved THz transmission spectroscopy of dielectrics. *Ferroelectrics*, 2000, **239**, 949–956.
17. Gervais, F., Infrared and millimeter waves Vol. 8. In *Chap. 7, High-temperature Infrared Reflectivity Spectroscopy by Scanning Interferometry*, ed. K. J. Button. Academic Press, New York, 1983, pp. 279–340.
18. Wakino, K., Murata, M. and Tamura, H., Far infrared reflection spectra of Ba(Zn,Ta)$O_3$-$BaZrO_3$ dielectric resonator material. *J. Am. Ceram. Soc.*, 1986, **69**, 34–37.
19. Gurevich, V. L., *Transport in Phonon Systems*. North Holland, Amsterdam, 1985.
20. Gurevich, V. L. and Tagantsev, A. K., Intrinsic dielectric loss in crystals. *Adv. Phys*, 1991, **40**, 719–767.
21. Petzelt, J. and Setter, N., Far infrared spectroscopy and origin of microwave losses in low-loss ceramics. *Ferroelectrics*, 1993, **150**, 89–102.
22. Petzelt, J., Kamba, S., Kozlov, G. V. and Volkov, A. A., Dielectric properties of microwave ceramics investigated by infrared and submillimetre spectroscopy. *Ferroelectrics*, 1996, **176**, 145–165.
23. Petzelt, J. and Kamba, S. *Proc. DRP'98, Szczyrk, Poland, September 1998, SPIE Proc.*, vol. 37DP, 1999, 227-234.
24. Petzelt, J. and Kamba, S. Submillimetre and infrared response of microwave materials: extrapolation to microwave properties. *Mat. Chem. Phys.* 2003, **79**, 175–180, and references therein.
25. Kozlov, G. and Volkov, A., Coherent source submillimeter wave spectroscopy (Millimeter and submillimeter wave spectroscopy). In *Topics in Current Chemistry*, ed. G. Gruner. Springer, Berlin, 1998, pp. 51–109.
26. Nilsen, W. G. and Skinner, J. G., Raman spectrum of strontium titanate. *J. Chem. Phys*, 1968, **48**, 2240–2248.